

Transition Metal-Based Thiometallates as Surface Ligands for Functionalization of All-Inorganic Nanocrystals

Hyewon Jeong, Sinmyung Yoon, Jung Hwa Kim, Do-Hyun Kwak, Da Hwi Gu, Seung Hwae Heo, Hyunhong Kim, Sangmin Park, Hyeong Woo Ban, Jongnam Park, Zonghoon Lee, Jong-Soo Lee, Kwangjin An, and Jae Sung Son

Chem. Mater., **Just Accepted Manuscript** • DOI: 10.1021/acs.chemmater.7b04387 • Publication Date (Web): 22 Nov 2017

Downloaded from <http://pubs.acs.org> on November 25, 2017

Just Accepted

“Just Accepted” manuscripts have been peer-reviewed and accepted for publication. They are posted online prior to technical editing, formatting for publication and author proofing. The American Chemical Society provides “Just Accepted” as a free service to the research community to expedite the dissemination of scientific material as soon as possible after acceptance. “Just Accepted” manuscripts appear in full in PDF format accompanied by an HTML abstract. “Just Accepted” manuscripts have been fully peer reviewed, but should not be considered the official version of record. They are accessible to all readers and citable by the Digital Object Identifier (DOI®). “Just Accepted” is an optional service offered to authors. Therefore, the “Just Accepted” Web site may not include all articles that will be published in the journal. After a manuscript is technically edited and formatted, it will be removed from the “Just Accepted” Web site and published as an ASAP article. Note that technical editing may introduce minor changes to the manuscript text and/or graphics which could affect content, and all legal disclaimers and ethical guidelines that apply to the journal pertain. ACS cannot be held responsible for errors or consequences arising from the use of information contained in these “Just Accepted” manuscripts.



Transition Metal-Based Thiometallates as Surface Ligands for Functionalization of All-Inorganic Nanocrystals

Hyewon Jeong,[†] Sinmyung Yoon,[‡] Jung Hwa Kim,[†] Do-Hyun Kwak,[§] Da Hwi Gu,[†] Seung Hwaee Heo,[†] Hyunhong Kim,[‡] Sangmin Park,[†] Hyeong Woo Ban,[†] Jongnam Park,[‡] Zonghoon Lee,[†] Jong-Soo Lee,[§] Kwangjin An,^{*,‡} and Jae Sung Son^{*,†}

[†]School of Materials Science and Engineering and [‡]School of Energy and Chemical Engineering, Ulsan National Institute of Science and Technology (UNIST), 50 UNIST-gil, Ulsan 44919, Republic of Korea.

[§]Department of Energy Systems Engineering, Daegu Gyeongbuk Institute of Science & Technology (DGIST), Daegu, 42988, Republic of Korea.

ABSTRACT: We report a new family of inorganic ligands, namely, transition metal-based thiometallates, for the surface functionalization of colloidal nanocrystals (NCs). We synthesized Pt-, Fe-, Co-, and Ni-based thiometallates, in which transition metal ions were complexed with polysulfides. These inorganic anions easily exchanged the surface organic ligands of various nanocrystals of metal, semiconductor, and oxide materials, without affecting the NCs' primary structural and optical characteristics. Furthermore, upon heating, these complexes were decomposed and transformed into crystalline phases of metal sulfides or pure metals, accompanied by the evaporation of S. Based on this effect, we selectively synthesized homogeneously distributed atomic Pt clusters or Pt nanoparticles on Fe₃O₄ nanomaterials by heating thioplatinate-capped Fe₃O₄ NCs. As a model application, we tested the prepared Pt-functionalized Fe₃O₄ nanomaterial as a heterogeneous catalyst for CO oxidation reaction and Pt-Fe₃O₄ catalysts exhibited the high turnover frequency due to the homogeneous distribution of atomic Pt over Fe₃O₄ and the corresponding strong metal-support interaction. This approach opens up a new avenue to functionalize nanocrystals for catalytic applications.

INTRODUCTION

Colloidally synthesized nanocrystals (NCs) have attracted tremendous attention in various disciplines, due to their monodispersity and tunable sizes and shapes, which determine their intrinsic electronic, optical, and magnetic properties.¹⁻³ Generally, the surfaces of colloidal NCs are sterically stabilized by organic capping ligands with long hydrocarbon chains (e.g., oleic acid, oleylamine, trioctylphosphine oxide), which play a key role during the formation of NCs in the synthesis stage and in ensuring easy dispersion of the prepared NCs in nonpolar organic media.⁴ However, these sterically bulky ligands sometimes block the access of foreign molecules. Therefore, post-treatments such as calcination are required to expose the surfaces of NCs for catalytic applications.⁵⁻⁷ Furthermore, the electrically insulating characteristics of organic ligands restrict the application of colloidal NCs in solid-state electronic devices.^{4,8} Hence, intensive research efforts are being devoted to designing surface ligands to provide new functionality to colloidal NCs and expand their application areas.^{4,9}

In recent years, surface ligands consisting of soluble anionic inorganic compounds have been developed for colloidal NCs.¹⁰ These inorganic ligands easily exchange the organic ligands on the surface of NCs to generate all-inorganic NCs, which exhibit dramatically enhanced device performance in arrays due to the strong electronic coupling. So far, various classes of inorganic ligands have been suggested: chalcogenidometallates,¹¹ metal-free anions¹²⁻¹⁴ (e.g. SCN⁻, S²⁻, Cl⁻), and oxoanions.¹⁵ Among these, chalcogenidometallates have been intensively studied using hydrazine-based chemistry due to their semiconducting functionality, by dissolving metal chalcogenide powders in hydrazine in the presence of excess chalcogens.¹⁶⁻¹⁹ While many classes of such materials could be prepared using this approach, however, the majority of the reported soluble chalcogenidometallates are based on post-transition metals including In, Ga, Sn, and Sb as the metal center, which restrict the application of all-inorganic NCs in electronic devices. Transition metal-based

chalcogenide ligands can open up new opportunities for all-inorganic NCs, since transition metals possess catalytic activity by having multiple oxidation states.²⁰⁻²² For example, atomic- to nano-scale transition metals on the surface of oxides can work well as supported heterogeneous catalysts,^{9,10} because of their high surface-to-volume ratio as most catalytic reactions occur on the surfaces. Recently, single-site atomic Pt on metal oxide support has gained significant attention in the field of catalysis, owing to the maximized use efficiency.²³⁻²⁷

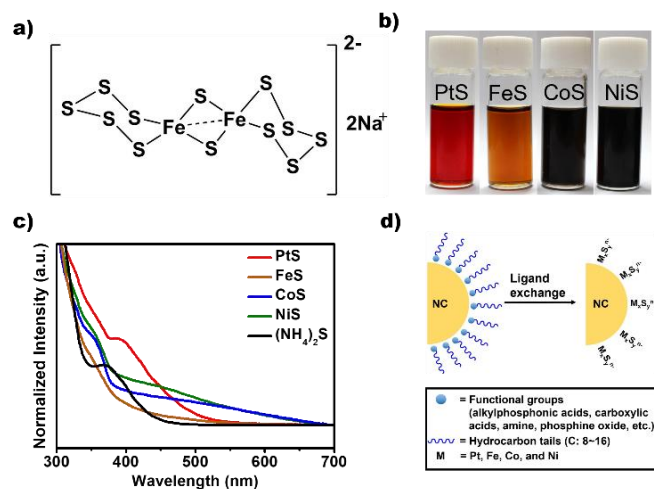


Figure 1. (a) Molecular structure of synthesized Na₂[FeS₆]₂. (b) Photographs showing synthesized thiometallates. (c) UV-Vis absorption spectra of transition metal-based thiometallates and (NH₄)₂S solutions. (d) Schematic illustration of the ligand exchange process with thiometallates.

Table 1. Nanocrystals, thiometallate ligands, and dispersible solvents for NCs capped with these ligands.

NCs	Thiometallates	Solvents
PbS, CdSe, CdS, FePt, Au, Bi,	(NH ₄) ₂ PtS ₁₅ , (NH ₄) ₂ CoS ₉ , (NH ₄) ₂ NiS ₆	NMF, DMF, DMSO, FA
	Na ₂ Fe ₂ S ₁₂ , (NH ₄) ₂ Fe ₂ S ₁₂	NMF, DMF
Fe ₃ O ₄	(NH ₄) ₂ PtS ₁₅ , Na ₂ Fe ₂ S ₁₂ , (NH ₄) ₂ Fe ₂ S ₁₂ , (NH ₄) ₂ CoS ₉ , (NH ₄) ₂ NiS ₆	DMF

In this work, we synthesized transition-metal based thiometallates containing Pt, Fe, Co, and Ni and systematically studied the general use of these anions as capping ligands for various colloidal NCs. To introduce transition metals for the metal centers, we revisited the old coordination chemistry²⁸⁻³⁰ where transition metal ions are directly reacted with polysulfide, instead of reducing bulk metal chalcogenide powders. The synthesized compounds were thiometallates, in which each transition metal ion is chelated with several sulfur atoms in polysulfides (Figure 1a and b). We also studied the heating-induced molecules-to-crystal transition in these thiometallates upon heating under various environments, which could introduce transition metal phases on oxide NC surfaces.

Next, we illustrate potential applications of this inorganic ligand chemistry for nano-catalysts. The combination of NC oxide support and transition metal-based ligands provides a great opportunity to design heterogeneous catalysts with transition metal active sites. For example, selective formation of atomic Pt clusters or Pt nanoparticles was achieved on Fe₃O₄ NCs after thermal treatment of thioplatinate-capped Fe₃O₄ NCs in air, and the products can be applied to various catalytic reactions such as oxygen-reduction reaction in fuel cells and water splitting. Accordingly, we applied our prepared materials for catalytic CO oxidation as a model reaction, and a high turnover frequency (TOF) was achieved.

EXPERIMENTAL SECTION

Materials. Ammonium sulfide solution ((NH₄)₂S, 40-48 wt% in H₂O, Aldrich), ammonium chloride (NH₄Cl, 99.0%, Samchun Chemical), amberlyst[®] 15 hydrogen form (Aldrich), cadmium oxide (CdO, ≥99.99%, Aldrich), borane *t*-butylamine complex (97%, Aldrich), chloroplatinic acid solution (H₂PtCl₆, 8 wt% in H₂O, Aldrich), trioctylphosphine oxide (TOPO, 99%, Aldrich), tetradecylphosphonic acid (TDPA, 97%, Aldrich), octadecylphosphonic acid (ODPA, 97%, Aldrich), selenium (powder, 99.99%, Aldrich), bismuth neodecanoate (technical grade, Aldrich), 1-octadecene (ODE, 90%, Aldrich), 1-dodecanethiol (DDT, 98%, Aldrich), trioctylphosphine (TOP, 90%, Aldrich), gold(III) chloride trihydrate (HAuCl₄·3H₂O, 99.9%, Aldrich), 1,2,3,4-tetrahydronaphthalene (tetralin, 97%, Alfa Aesar), iron chloride (FeCl₂, 98%, Aldrich), Iron(III) chloride hexahydrate (ACS reagent, 97%), sodium oleate (≥82%, Aldrich), nickel(II) acetate tetrahydrate (98%, Aldrich), nitrosonium tetrafluoroborate (NOBF₄, 97%, Acros), cobalt(II) acetate tetrahydrate (reagent grade, Aldrich), sodium (ACS reagent, dry, Aldrich), platinum(II) acetylacetonate (Pt(acac)₂, 99.99%, Aldrich), iron(III) acetylacetonate (Fe(acac)₃, 99.95%, Aldrich), octyl ether (99%, Aldrich), 1,2-Hexanedecanediol (90%, Aldrich), oleylamine (OAm, approximate C18-content 80-90%, Acros organics), oleic acid (OA, 90%, Aldrich), tetraethylammonium bromide (TEAB, 99%, Aldrich), cadmium

chloride (99.99%, Aldrich), sulfur (99.998%, Aldrich), octylamine (99%, Aldrich), lead(II) chloride (PbCl₂, reagent grade 99%, Alfa Aesar) were used as received.

Synthesis of thiometallate.

Thioplatinate complex was prepared according to the procedure reported by Wickenden *et al.*²⁸ with modifications in reaction time and purifying solvents. 5 mL of (NH₄)₂S 45-48 wt% aqueous solution was diluted with 5 mL of distilled water while stirring. 3.0 g of sulfur was added to the mixture and stirred until it became clear red solution. 1.25 mL of chloroplatinic acid solution was then added dropwise to the polysulfide solution. It was then stirred until the solution became turbid. The mixture was precipitated by centrifugation and the precipitates were purified with a small amount of methanol (MeOH) and excess toluene for three times. The final product was re-dispersed in 10 mL of *N*-Methylformamide (NMF) or *N,N*-Dimethylformamide (DMF) and filtered with a 0.20 μL PTFE filter.

Thioferrite complex was synthesized following the procedure reported by Strasdeit *et al.*²⁹ with modifications as follows. In a N₂-filled glove box, FeCl₂ (1 mmol), sulfur (6 mmol), and sodium (3 mmol) in 5 mL of DMF were stirred at 70 °C for 6 hours and cooled to RT. 3 mL of methanol (MeOH) was then added to the mixture and was precipitated by centrifugation (at 4000 rpm for 3 min). The supernatant was stirred with excess MeOH (up to 40-50 mL) overnight. It was then precipitated by centrifugation at 7000 rpm for 10 min. The precipitates were purified with 10 mL of MeOH followed by centrifugation for two times. The final product was re-dispersed in NMF and was further used after filtering with a 0.20 μL PTFE filter.

Thionickelate complex was synthesized according to the procedure reported by Müller *et al.*³⁰ with modifications in polysulfide solution. 5 mL of (NH₄)₂S solution (45-48 wt%) was diluted with H₂O to a 50 % solution and 1g of sulfur was added to the solution. 0.8 g of TEAB was dissolved in 10 mL of the mixture. 0.4 g of nickel(II) acetate tetrahydrate was then added step-wise and the mixture was heated to 45 °C while stirring. As it reached the temperature, the mixture was quickly precipitated by centrifugation at 4000 rpm for 3 min. The supernatant was kept in a closed conical tube for an hour. No crystals were observed. The mixture was then purified using 2-propanol (IPA) and methanol (MeOH) for three times and was finally dispersed in 10 mL of NMF or DMF.

Thiocobaltate complex was synthesized by using a slightly modified procedure from the synthesis of thionickelate. The ammonium sulfide aqueous solution was diluted to half with MeOH since cobalt precursor possessed higher solubility in MeOH than water. 0.38 g of cobalt (II) acetate tetrahydrate was added step-wise and the solution was stirred at 50 °C. As it reached the temperature, the mixture was quickly precipitated by centrifugation at 4000 rpm for 3 min. The supernatant was kept in a closed conical tube for an hour. No crystals were observed. The mixture was then purified using excess 2-propanol

(IPA). The final solution was dispersed in 10 mL of either NMF or DMF.

The cation exchange from Na^+ to NH_4^+ or vice versa was conducted following the procedure described in the literature reported by Zhang *et al.*¹⁴ Acid beads (Amberlyst® 15 hydrogen form, Aldrich) was immersed in 30 mL of NH_4Cl (0.2 M~0.3 M, pH: ~4-5) and sonicated for over 10 min. Resin-beads were collected after centrifugation. The pH value of the supernatant almost reached ~2. The beads were dried under vacuum after washing with D.I water. The NCs capped with thioferrite ligand was dispersed in NMF. This mixture was vigorously vortexed with NH_4^+ -resin for 15-20 min. It was then precipitated by centrifugation and washed with toluene. The final product was dispersed in 10 mL of NMF or DMF.

Synthesis of organics-capped NCs.

16-20 nm-sized Fe_3O_4 NCs were synthesized by the method reported by Park *et al.*³¹ In a typical synthesis, iron oleate (10 mmol), and oleic acid (7 mmol) were dissolved in 30 g of 1-octadecene. The mixture was heated to 320 °C for 30 min with a heating rate of 3.3 °C/min and was cooled to RT under inert atmosphere. The product was collected using ethanol by centrifugation and was dispersed in hexane.

6.7 nm-sized PbS NCs were synthesized according to the reported literature by Weidman *et al.*³² with slight modifications. The sulfur precursor was prepared by using a heating mantle with a heating rate of 5 °C/min for 20 min. As it reached 120 °C, the orange and amber-like mixture was cooled to RT.

6.0 nm-sized Au NCs were synthesized following the reported literature by Zhu *et al.*³³ with a few modifications. Here, the 0.2 g of HAuCl_4 was dissolved in 10 mL of tetralin and 10 mL of oleylamine at room temperature under N_2 flow.

11 nm-sized Bi NCs were synthesized according to the method developed by Son *et al.*³⁴ with slight alterations. Acetone was only used as anti-solvent instead of tetrahydrofuran (THF).

1.2 nm-thick CdS nanoplates were synthesized following the same experimental procedure reported by Son *et al.*³⁵

2.5 nm-sized FePt NCs were synthesized following the same experimental procedure reported by Liu *et al.*³⁶

CdSe NCs capped with ODPa were prepared according to previously reported procedures.³⁷

Ligand exchange with thiometallate.

The ligand exchange process was conducted in a N_2 -filled glovebox. Thiometallate complexes was dispersed in 7~10 mL of NMF. For the typical ligand exchange process, 2 mL of ligand solution formed the bottom layer and the NCs dispersed in hexane formed the upper layer. This two-phase mixture was vigorously stirred for at least 30 min until the upper layer became clear as shown in Figure S1. The transferred phase into the bottom layer was purified with IPA (NMF:IPA ~ 1:3) when the exchanging ligands were thioplatinate and thioferrite. Instead of IPA, acetonitrile was used as purifying solvent for the rest of thiometallate ligands (NMF:ACN ~ 1:0.5). The mixture was precipitated by centrifugation (13,000 rpm, 5 min) for more than three times. The possible final dispersants are summarized in Table 1. The ligand exchange process for Fe_3O_4 NCs was performed by modified two-step method from the literature reported by Dong *et al.*³⁸ The organics- Fe_3O_4 was dispersed in hexane and formed the upper layer and 120 mg of NOBF_4 dispersed in 2 mL of DMF formed the bottom layer. It was then stirred overnight. The ligand stripped Fe_3O_4 was washed with

toluene (DMF:Toluene = 1:2) for two times and was finally dispersed in DMF. Meanwhile, the thioplatinate ligand solution was dispersed in DMF and followed by filtration. Each solution was then mixed together and sonicated for the interaction between slightly positive surface charge over Fe_3O_4 and the anionic thioplatinate ligand.

Characterization. Transmission electron microscopy (TEM) images of nanocrystals (NCs) were collected using a JEOL-2100 instrument operated at 200 kV. The samples dispersed in non-polar solvents were prepared by drop-casting on carbon-coated TEM grids and dried under air while the samples dispersed in polar solvents were dried under vacuum. STEM-EDS and HAADF-STEM characterization was conducted in a Cs probe aberration-corrected FEI Titan Cube TEM with an electron monochromator operated at 80 kV. X-ray diffraction (XRD) patterns were obtained using a Rigaku D/Max2500V diffractometer equipped with a Cu-rotating anode X-ray source. Electronic states of Pt species were obtained using a ThermoFisher K-alpha X-ray photoelectron spectrometer. The absorption spectra of colloidal NCs and ligands were acquired using a Cary 5000 UV-Vis-NIR spectrophotometer. Photoluminescence (PL) spectra of colloidal solutions in the wavelength range of 500-700 nm were obtained using a Cary Eclipse fluorescence. Fourier transform infrared (FT-IR) spectra were obtained in ATR mode using a 670/620 varian FT-IR spectrometer with averaging over 32 scans. ζ -potential data were collected using a Malvern Zetasizer Nano-ZS90. Elemental analysis by inductively coupled plasma optical emission spectrometers (ICP-OES) was carried out using a varian 700-ES. Thermogravimetric analysis (TGA) was conducted using a TA-Q500 thermal analyzer with a heating rate of 10 °C/min under air or under nitrogen.

RESULTS AND DISCUSSION

The synthesis of Pt-, Co-, and Ni-based thiometallates was conducted using a modified version of the reported synthetic route for thioplatinate.²⁸ Typically, aqueous solutions of metal ions were reacted with ammonium polysulfide at near room temperature. Thioferrite was synthesized by an alternative route in which FeCl_2 precursor was reacted with elemental S in the presence of Na as a reducing agent.²⁹ The produced thiometallates had $(\text{NH}_4)^+$ or Na^+ as counter ions, which could be exchanged by a cationic exchange reaction. The metal-to-sulfur ratio spans a large range depending on the metal center. For example, this ratio in thioferrite and thioplatinate analyzed by inductively coupled plasma optical emission spectroscopy (ICP-OES) is 1:6 and 1:15, respectively, corresponding to literature values.^{28,29} On the other hand, thiocobaltate and thionickelate synthesized by the modified route for thioplatinate showed the respective ratios of 1:9 and 1:6. The synthesized compounds were characterized by UV-Vis absorption spectroscopy. As shown in Figure 1c, thioplatinate and thioferrite exhibited absorption peaks at 391 and 351 nm, respectively. Thiocobaltate and thionickelate also displayed broad absorption bands throughout the visible region with peaks at 360 nm. These peaks are completely different from that observed in the spectrum of $(\text{NH}_4)_2\text{S}$ (a single peak at 372 nm), demonstrating the formation of thiometallates.

The ligand exchange of organics-capped NCs with the current thiometallates was conducted using a typical two-phase reaction (Figure 1d). We studied a variety of combinations of NCs (such as semiconductors, metals, and oxides) and thiometallate ligands. This two-phase reaction worked very well for PbS,

CdSe, CdS, Au, FePt, and Bi (Figure 3a and Figure S1 in Supporting Information). Regardless of the NCs and thiometallate ligands, all NCs exhibited negative zeta (ζ) potentials after ligand exchange. For example, the thiometallate-capped PbS NCs showed ζ potentials that ranged from -10.0 to -31.4 mV, demonstrating the attachment of thiometallates on the NC surface (Figure 2a). On the other hand, we found that Fe₃O₄ NCs dispersed in hexane were not transferred into the polar phase. Huang, *et al.* reported that ligand exchange of NCs with less nucleophilic anions can be achieved by a two-step procedure: stripping the organic capping ligand with tetrafluoroborate followed by the attachment of inorganic ligands on the NC surface.^{15,38} We conducted similar two-step reactions for the ligand exchange of Fe₃O₄ NCs to obtain stable colloidal solutions of thiometallate-capped Fe₃O₄ NCs in *N,N*-dimethylformamide (DMF) (Figure S2). The ζ potentials of ligand-stripped Fe₃O₄ and PtS-Fe₃O₄ are shown in Figure 2b, as +19.4 and -11.6 mV, respectively, demonstrating the attachment of negatively charged thiometallates. All studied combinations of NCs and thiometallate ligands are summarized in Table 1.

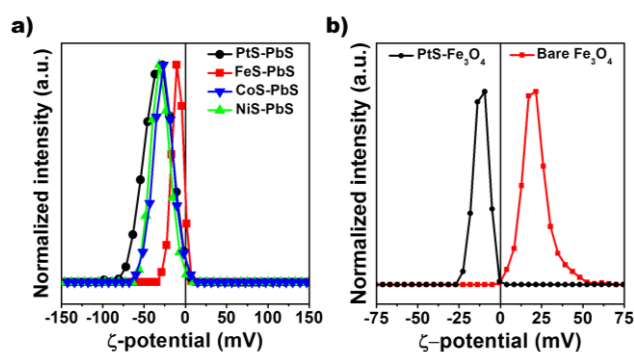


Figure 2. ζ potentials measured for (a) thiometallates-capped PbS NCs in NMF, and (b) ligand-stripped and thiomplatinate-capped Fe₃O₄ NCs in DMF.

Transmission electron microscopy (TEM) images were obtained for the primary organics-capped spherical NCs of CdSe, PbS, Au, FePt, Bi, and Fe₃O₄, after exchange with various thiometallate capping ligands (Figure 3 and Figure S3-S5). Figures 3b-3e, S3, and S4 reveal that the ligand exchange reactions did not affect the size and shape of NCs, except for Fe₃O₄. In the case of Fe₃O₄, the ligand-stripping step seemed to etch the surface of NCs and reduce their size (Figure S5a,b), which can be attributed to its oxidative properties and Lewis acidity of the nitrosonium cation. However, the thiometallate attachment step did not affect the size or shape of Fe₃O₄ NCs, as confirmed by TEM analysis (Figure S5b,c). To test the applicability of these ligands for NCs with different shapes, ultrathin CdS nanoplates with a thickness of 1.2 nm were also utilized for the exchange with PtS ligands. According to the TEM image (Figure S4d), the CdS nanoplates retained their ultrathin characteristics afterwards.

Optical properties of thiometallate-capped CdSe NCs and CdS nanoplates were investigated by UV-Vis absorption and photoluminescence (PL) spectroscopy. The CdSe NCs showed identical spectra with either thiometallate- or primary organics-capping (Figure 4a), which demonstrates that the ligand exchange process did not affect the structural and electronic characteristics of these CdSe NCs. The CdS nanoplates also showed very similar absorption spectra after the ligand exchange. The only change was that the peak became broader and red-shifted with

the thioplatinate-capped CdS nanoplates (Figure 4b), which can be attributed to the electronic coupling between the exciton states of CdS nanoplates and thioplatinate, since thioplatinate has a strong absorption band at 391 nm (Figure 1c). On the other hand, the emission properties of CdSe NCs almost disappeared after the ligand exchange process (Figures 4c and S6). The observed PL quenching phenomenon on CdSe NCs after the ligand exchange reaction can be attributed to the formation of multiple surface defects on NCs, which agrees with the previous studies on inorganic ligand-capped CdSe NCs.³⁹ Recently, our group reported the recovery of PL properties of all-inorganic NCs via a photo-oxidation process, in which a robust oxidized surface is formed on NCs to cure the surface defects.³⁹ Likewise, we performed the photo-oxidation treatment on PtS, FeS, CoS, NiS thiometallates-capped CdSe NCs (Figure 4c and Figure S6). The PL spectra showed greatly enhanced emission properties in all cases, and these observations are in agreement with those of previously reported MoS₄²⁻ and WS₄²⁻-capped CdSe NCs.³⁹ Unlike other NCs, the PL peak position of thioferrite-capped CdSe NCs was shifted to a lower wavelength (Figure S6a), which indicates the reduction in the NC size. This shift can be attributed to the etching effect from residual Cl⁻ ion in thioferrite, since the precursor for thioferrite was FeCl₂. In our previous report, a significant blue shift was also observed in the PL spectrum of Cl⁻-capped CdSe NCs after the photo-oxidation process.³⁹

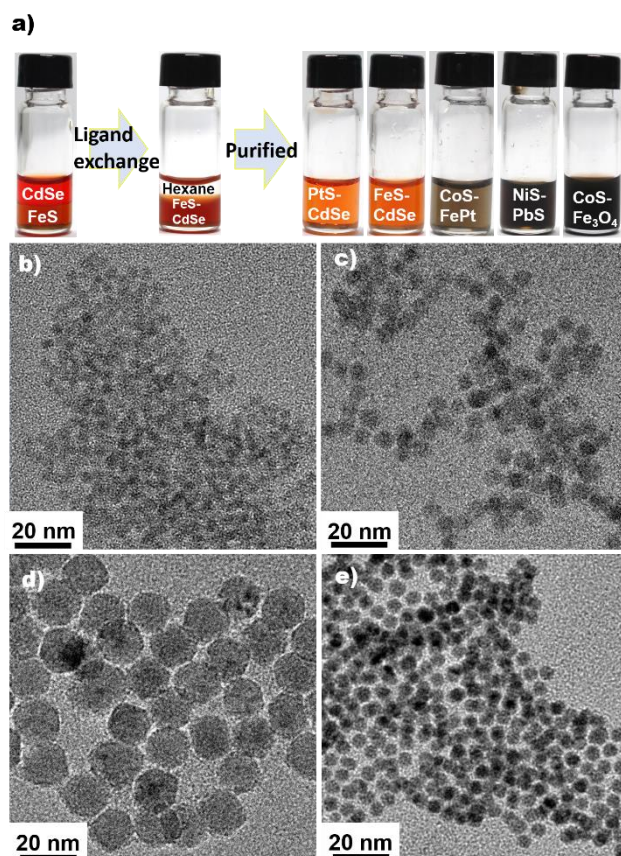


Figure 3. (a) Photographs showing the ligand exchange process. TEM images of NCs: (b) PtS-capped CdSe (size: 4.6 nm), (c) FeS-capped PbS (6.7 nm), (d) CoS-capped Fe₃O₄ (16 nm), and (e) NiS-capped Au (6.0 nm).

The degree of ligand exchange on PbS and CdSe NCs capped with thiometallates was studied by Fourier transform infrared

absorption (FT-IR) spectroscopy. As shown in Figure 4d, the absorption bands of C-H stretching modes (2700–3000 cm^{-1}) were observed in the organic-capped NCs but not in the thiometallate-capped ones (Figure 4d), suggesting the complete replacement of the organic ligands with inorganic thiometallates. The surface coverage of thiometallate ligands on PbS (particle size: 6.7 nm) was estimated with ICP-OES, and all ligands were found to have surface coverages in the range of 14–30%. These values are in agreement with the result reported for typical inorganic ligands.³⁹

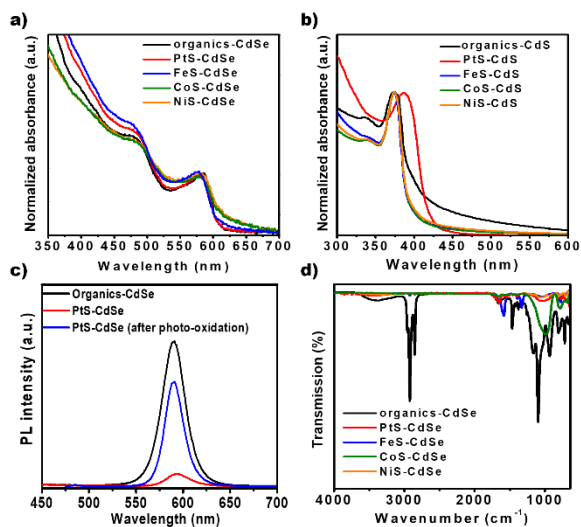


Figure 4. UV-Vis absorption spectra of organics- and thiometallate-capped (a) CdSe NCs and (b) CdS nanoplates. (c) PL spectra of organics-capped CdSe and PtS-capped CdSe NCs before and after photo-oxidation. (d) FT-IR spectra of organics- and thiometallates-capped CdSe NCs.

Generally, chalcogenidometallate compounds synthesized by the hydrazine- or mixed solvent-reducing route from metal chalcogenide powders can decompose back into crystalline semiconducting metal chalcogenides upon heat treatment.^{17,18} This effect has been intensively studied for solution-processed fabrication of semiconductor thin films using chalcogenidometallate inks. Thus, the current thiometallates were analyzed by thermogravimetric analysis (TGA) under N_2 and air environments, and XRD analysis before and after heating. All TGA data showed a remarkable weight loss at 150–300 $^{\circ}\text{C}$ under both N_2 and air environments, depending on the type of thiometallate (Figure S7). Therefore, these compounds thermally decompose into crystalline phases in a manner similar to that previously described for typical chalcogenidometallates.^{16,17} At above 300 $^{\circ}\text{C}$, a slight weight loss was observed under both N_2 and air, and tentatively attributed to S evaporation from the formed metal sulfides.

XRD patterns of thioferrite and thionickelate annealed at 300 $^{\circ}\text{C}$ show sharp crystalline peaks that can be indexed as cubic FeS_2 (JCPDS 00-042-1340) and cubic NiS_2 (JCPDS 03-065-3325) structures (Figures 5a and 5b). At the annealing temperature of 500 $^{\circ}\text{C}$, thioferrite was transformed into the mixed phases of FeS (JCPDS 03-065-9124(RDB)) and FeS_2 , indicating the evaporation of S. Also, the XRD pattern of thionickelate at 500 $^{\circ}\text{C}$ matches those of both Ni (JCPDS 00-004-0850) and NiS (JCPDS 03-065-5762) phases. In thiocobaltate, the sample annealed at 300 $^{\circ}\text{C}$ might be amorphous because there were no

pronounced XRD peaks, while a crystalline phase corresponding to the hexagonal CoS (JCPDS 03-065-8977) was observed in the pattern after annealing at 500 $^{\circ}\text{C}$ (Figure 5c). It is noteworthy that thioplatinate exhibits broad peaks that do not correspond to any related references when heated under N_2 even up to 500 $^{\circ}\text{C}$ (Figure 5d), whereas a pure Pt crystalline phase appears upon annealing at temperatures above 300 $^{\circ}\text{C}$ under air (Figure 6a). This transformation should be due to the sulfur oxidation and subsequent evaporation of SO_x during the heat treatment. Other thiometallates were transformed into metal sulfate phases (Figure S8) under air. These results demonstrate the applicability of the current thiometallates as precursors for introducing transition metal sulfides or pure metals on the surfaces of desired materials.

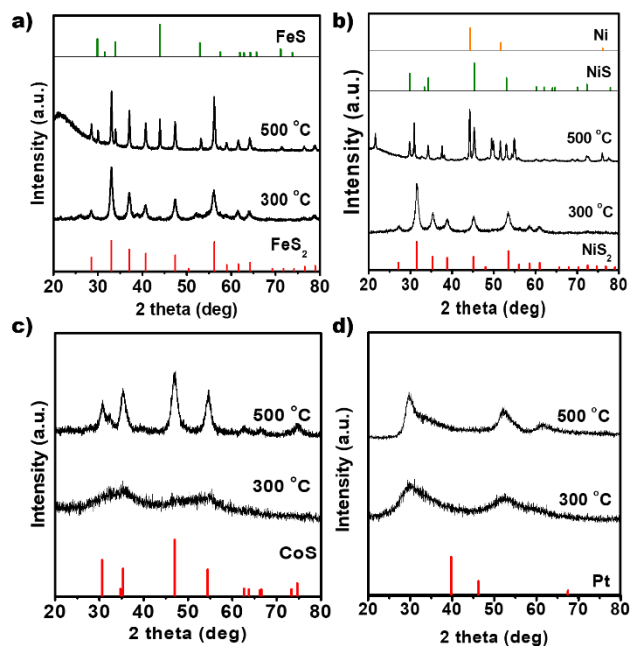


Figure 5. XRD patterns of (a) thioferrite, (b) thionickelate, (c) thiocobaltate, and (d) thioplatinate annealed at various temperature under N_2 environment. The vertical lines show the patterns of references.

To study the structural transformations of these thiometallates on the NC surfaces, we investigated the annealing behaviors of thiometallate-capped Fe_3O_4 NCs and organics-capped Fe_3O_4 NCs by thermogravimetric analysis (TGA), since Fe_3O_4 NCs have sufficiently high thermal stability to exclude possible side reactions between NCs and ligands. As shown in Figure S9, all TGA spectra of thiometallate-capped Fe_3O_4 NCs shows a weight loss of 6–15% at 150–300 $^{\circ}\text{C}$, indicating the thermal decomposition of thiometallates on NCs. Furthermore, the degree of a weight loss in the TGA spectra is in order of thiocobaltate, thioplatinate, thionickelate, and thioferrite, which agrees with the TGA data of thiometallates. On the other hand, organics-capped Fe_3O_4 NCs exhibit two distinct weight losses at ~ 250 $^{\circ}\text{C}$ and ~ 380 $^{\circ}\text{C}$, agreeing with the previously reported TGA result of oleic acid-capped Fe_3O_4 NCs. Zhang, et al. claimed that these two transitions might stem from the evaporation of oleic acid capping on two different crystalline facets.⁴⁰

We further studied thioplatinate-capped Fe_3O_4 NCs since Pt is an important catalytic element. The XRD pattern of the thioplatinate-capped Fe_3O_4 NCs was almost identical after heat

treatment, with slight peak sharpening arising from partial agglomeration (Figure 6b). At the same time, we could not observe any peaks arising from the thioplatinate, meaning that no crystalline domains of Pt formed that were detectable by XRD. TEM analysis (Figure 6c) reveals that the size and shape of the thioplatinate-capped Fe_3O_4 NCs barely changed during annealing. Elemental mapping image obtained by energy dispersive spectroscopy (EDS) (Figure 6c) shows homogeneous distribution of Pt on the surface of Fe_3O_4 NCs. Also, we did not observe any Pt nanoparticles in the TEM analysis, which was consistent with the absence of Pt peaks in the XRD pattern. We further characterized the configuration of the Pt on Fe_3O_4 NCs by high-angle annular dark field (HAADF) scanning transmission electron microscopy (STEM). The HAADF-STEM image displays well-distributed atomic Pt clusters showing different contrast at the edge of Fe_3O_4 NCs (Figure 6d). Pt clusters with size of less than 2 nm were clearly observed, indicating that single Pt atoms^{26,27} were incorporated into the Fe_3O_4 lattices homogeneously.

We further heated the thioplatinate-capped Fe_3O_4 in the presence of excess thioplatinate under the same condition. The XRD pattern shown in Figure 7a demonstrates the formation of a Pt phase together with Fe_3O_4 NCs. The TEM image also shows that Pt nanoparticles with an average size of 3.3 nm were formed on the surface of Fe_3O_4 NCs, which were further confirmed by TEM-EDS mapping analyses (Figures 7c, S10, and S11).

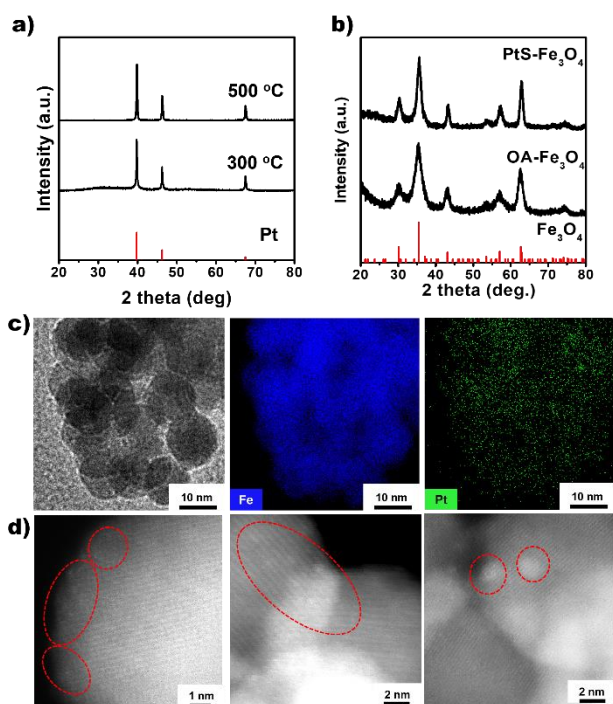


Figure 6. (a) XRD patterns of thioplatinate compound annealed at 300 °C and 500 °C in air. (b) XRD patterns of as-synthesized organics-capped Fe_3O_4 and annealed thioplatinate-capped Fe_3O_4 NCs at 500 °C. (c) TEM-EDS mapping and (d) HAADF-STEM images of Pt-decorated Fe_3O_4 .

Both Pt atomic clusters- and Pt nanoparticles-decorated Fe_3O_4 samples were analyzed by X-ray photoelectron spectroscopy (XPS). The XPS spectrum of Fe_3O_4 with Pt atomic clusters shows multiple peaks assignable to Pt^0 , Pt^{2+} , and Pt^{4+} (Figure

8a), suggesting the formation of Pt single atoms in the oxide lattice as a result of the partially vacant 5d orbitals.²⁴ The XPS spectrum of the Pt nanoparticles on Fe_3O_4 confirms that the nanoparticles consisted of the fully reduced metallic phase Pt^0 (Figure 8b). Similarly, in the previous report by Huang *et al.*, XPS spectra of dendrimer-encapsulated Pt clusters with the Pt size of less than 1 nm indicated that 93% of the Pt was oxidized, while Pt nanoparticles with sizes above 2.5 nm exhibited metallic Pt phase in the XPS.⁴¹ These results reveal the controllable formation of Pt atoms and nanoclusters with different sizes and chemical states on the surface of oxide NCs (Figure 8c).

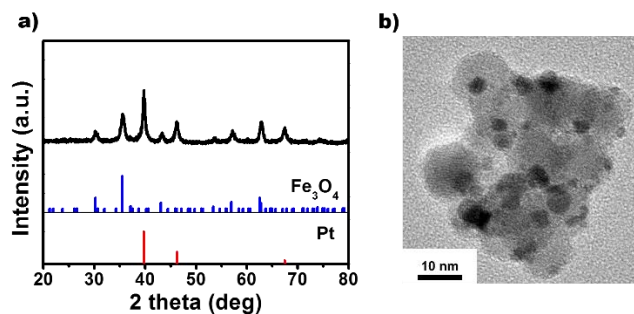


Figure 7. (a) XRD pattern and (b) TEM image of thioplatinate-capped Fe_3O_4 NCs annealed with excess thioplatinate at 500 °C.

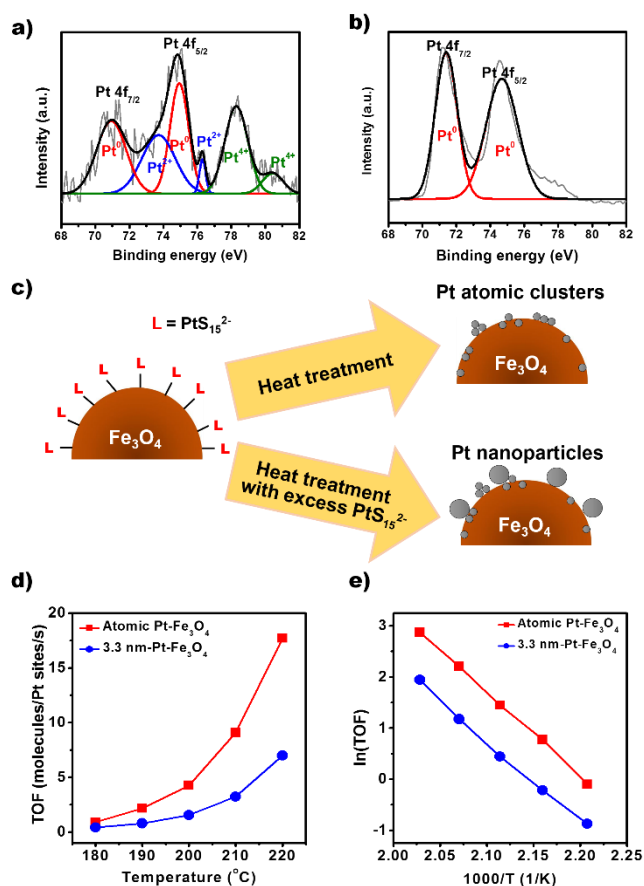


Figure 8. XPS spectrum of (a) Pt atomic clusters and (b) Pt nanoparticles on Fe_3O_4 NCs. (c) Scheme for the formation of a Pt phase on NCs. (d) Turnover frequencies and (e) Arrhenius plots of the atomic Pt- Fe_3O_4 and the 3.3 nm-sized Pt- Fe_3O_4 catalysts for CO oxidation in the temperature range of 180 °C-220 °C

Finally, as a model application, we carried out CO oxidation over the prepared Pt nanocatalysts supported on Fe₃O₄. Two Pt-Fe₃O₄ catalysts with Pt atoms and 3.3-nm Pt nanoparticles were compared in a batch reactor under 40 Torr CO, 100 Torr O₂, and 620 Torr He in the temperature range of 180–220 °C. The TOFs were determined from the rate of CO oxidation normalized by the number of Pt active sites on the oxide NC surfaces, as determined by ethylene hydrogenation.⁵ The loading of Pt per Fe₃O₄ measured by ICP-OES was 1.18 and 14.0 % for the atomic Pt-Fe₃O₄ and the 3.3 nm-Pt on Fe₃O₄, respectively. Figures 8d and 8e show the TOFs of Pt-catalyzed CO oxidation as a function of the reaction temperature, and the activation energies from the Arrhenius plots. The obtained TOFs clearly confirm that active Pt sites were successfully created on the surface of Fe₃O₄ NCs. Although the Pt nanoparticles-Fe₃O₄ had a higher Pt loading, the atomic Pt-Fe₃O₄ exhibited CO oxidation rates that are more than two times higher. The TOFs shown in the present work are higher than the reported values of commercial Pt-Al₂O₃, Pt nanoparticles, and Pt nanoparticles on various support oxides.^{6,42,43} This enhancement of the TOF in the atomic Pt-Fe₃O₄ can be understood by several mechanism. First, atomic Pt catalytic sites on Fe₃O₄ can be more reactive than catalytic sites of Pt nanoparticles on Fe₃O₄. Qiao, et al. demonstrated that the more vacant d orbitals of the charged single Pt atoms help to reduce the CO adsorption energy as well as the activation barriers for CO oxidation.²⁶ However, in this work, the activation barrier for CO oxidation was almost identical in both atomic Pt and 3.3 nm-sized Pt on Fe₃O₄ (Table S1), which distinguishes the catalytic reaction pathway in atomic Pt-Fe₃O₄ in this work from the previously reported one. Secondly, the contact of Pt on Fe₃O₄ may affect the catalytic activity. Previous studies reported that CO oxidation rate was increased in the presence of oxide support due to the strong metal-support interaction between Pt and oxide.⁴⁴ As shown in the XPS spectrum (Figure 8a), atomic Pt was incorporated on the surface of Fe₃O₄ and this could be responsible for the stronger metal support interaction between Pt and Fe₃O₄, resulting in the high TOF. On the other hand, in the case that the size of Pt was increased to 3.3 nm, it was speculated that the metal-support interaction was weakened with the strong metallic character of Pt, confirmed by the XPS analysis (Figure 8b). Moreover, the homogeneous distribution of atomic Pt over Fe₃O₄ might further contribute to increase the TOF.

CONCLUSION

In summary, we have shown the general applicability of transition metal-based thiometallates of PtS, FeS, CoS, and NiS as ligands for colloidal NCs. These inorganic anions as ligands could stabilize NC colloids, while preserving the properties of the primary NCs. Furthermore, upon heat treatment, the structural transformation in the thiometallates from molecules to crystals enabled us to prepare nanostructures decorated with atomic or nano-scale transition metals or transition metal sulfides, which can display catalytic activity. Specifically, we selectively synthesized atomic or nanoscale Pt-decorated Fe₃O₄ as a heterogeneous catalyst for CO oxidation. The Pt-decorated Fe₃O₄ showed greatly enhanced CO oxidation rate, as a result of the atomic distribution of Pt over the surface of Fe₃O₄. Our results not only add to the understanding of surface chemistry of colloidal NCs, but also unveil a synthetic route for all-inorganic NCs capped with transition metal-based ligands for new catalytic applications.

ASSOCIATED CONTENT

Supporting Information. Solution photographs before and after the ligand exchange, scheme for two-step ligand exchange, TEM images of NCs before and after the ligand exchange, PL spectra of NCs, TGA spectra and XRD patterns of thiometallates, size histogram of Pt nanoparticles, TEM-EDS mapping image of Pt nanoparticles, and TOFs and activation energy of CO oxidation.

AUTHOR INFORMATION

Corresponding Author

kjan@unist.ac.kr (K.A.) & jsson@unist.ac.kr (J.S.S.)

ACKNOWLEDGMENT

This research was supported by the Nano-Material Technology Development Program (No. 2016M3A7B4900044) (J.S.S.) and Basic Science Research Program (No. 2015R1C1A1A01055092) (K.A.) through the National Research Foundation of Korea (NRF) funded by the Ministry of Education, and the 2015 Research Fund (1.150109.01) of UNIST (K.A.).

ABBREVIATIONS

NCs, Nanocrystals; NMF, *N*-Methylformamide; DMF, *N,N*-Dimethylformamide, ACN, Acetonitrile.

REFERENCES

- Yin, Y.; Alivisatos, A. P. Colloidal Nanocrystal Synthesis and the Organic-Inorganic Interface. *Nature* **2005**, *437*, 664-670.
- Park, J.; Joo, J.; Kwon, S. G.; Jang, Y.; Hyeon, T. Synthesis of Monodisperse Spherical Nanocrystals. *Angew. Chem. Int. Ed.* **2007**, *46*, 4630-4660.
- Pileni, M. P. The Role of Soft Colloidal Templates in Controlling the Size and Shape of Inorganic Nanocrystals. *Nat. Mater.* **2003**, *2*, 145-150.
- Boles, M. A.; Ling, D.; Hyeon, T.; Talapin, D. V. The Surface Science of Nanocrystals. *Nat. Mater.* **2016**, *15*, 141-153.
- Kuhn, J. N.; Tsung, C. K.; Huang, W.; Somorjai, G. A. Effect of organic capping layers over monodisperse platinum nanoparticles upon activity for ethylene hydrogenation and carbon monoxide oxidation. *J. Catal.* **2009**, *265*, 209-215.
- Park, J. Y.; Aliaga, C.; Renzas, J. R.; Lee, H.; Somorjai, G. A. The Role of Organic Capping Layers of Platinum Nanoparticles in Catalytic Activity of CO Oxidation. *Catal. Lett.* **2009**, *129*, 1-6.
- Aliaga, C.; Park, J. Y.; Yamada, Y.; Lee, H. S.; Tsung, C. K.; Yang, P. D.; Somorjai, G. A. Sum Frequency Generation and Catalytic Reaction Studies of the Removal of Organic Capping Agents from Pt Nanoparticles by UV-Ozone Treatment. *J Phys Chem C* **2009**, *113*, 6150-6155.
- Talapin, D. V.; Murray, C. B., PbSe nanocrystal solids for n- and p-channel thin film field-effect transistors. *Science* **2005**, *310*, 86-89.
- Medintz, I. L.; Uyeed, H. T.; Goldman, E. R.; Mattoussi, H. Quantum Dot Bioconjugates for Imaging, Labelling and Sensing. *Nat. Mater.* **2005**, *4*, 435-446.
- Nag, A.; Zhang, H.; Janke, E.; Talapin, D. V., Inorganic surface ligands for colloidal nanomaterials *Z. Phys. Chem.* **2015**, *229*, 85-107.
- Kovalenko, M. V.; Scheele, M.; Talapin, D. V. Colloidal Nanocrystals with Molecular Metal Chalcogenide Surface Ligands. *Science* **2009**, *324*, 1417-1420.

- (12) Fafarman, A. T., *et al.* Thiocyanate-Capped Nanocrystal Colloids: Vibrational Reporter of Surface Chemistry and Solution-Based Route to Enhanced Coupling in Nanocrystal Solids. *J. Am. Chem. Soc.* **2011**, *133*, 15753-15761.
- (13) Nag, A.; Kovalenko, M. V.; Lee, J. S.; Liu, W.; Spokoyny, B.; Talapin, D. V. Metal-Free Inorganic Ligands for Colloidal Nanocrystals: S^{2-} , HS^- , Se^{2-} , HSe^- , Te^{2-} , HTe^- , TeS_3^{2-} , OH^- , and NH_4^+ as Surface Ligands. *J. Am. Chem. Soc.* **2012**, *134*, 13604-10620.
- (14) Zhang, H.; Jang, J.; Liu, W.; Talapin, D. V. Colloidal Nanocrystals with Inorganic Halide, Pseudohalide, and Halometallate Ligands. *ACS Nano* **2014**, *8*, 7359-7369.
- (15) Huang, J.; Liu, W.; Dolzhenkov, D. S.; Protesescu, L.; Kovalenko, M. V.; Koo, B.; Chattopadhyay, S.; Shenchenko, E. V.; Talapin, D. V. Surface Functionalization of Semiconductor and Oxide Nanocrystals with Small Inorganic Oxoanions (PO_4^{3-} , MoO_4^{2-}) and Polyoxometalate Ligands. *ACS Nano* **2014**, *8*, 9388-9402.
- (16) Mitzi, D. B. Solution Processing of Chalcogenide Semiconductors via Dimensional Reduction. *Adv. Mat.* **2009**, *21*, 3141-3158.
- (17) Webber, D. H.; Brutchey, R. L. Alkahest for V2V3 Chalcogenides: Dissolution of Nine Bulk Semiconductors in a Diamine-Dithiol Solvent Mixture. *J. Am. Chem. Soc.* **2013**, *135*, 15722-15725.
- (18) McCarthy, C. L.; Brutchey, R. L. Solution Processing of Chalcogenide Materials using Thiol-Amine "alkahest" Solvent Systems. *Chem. Commun.* **2017**, *53*, 4888-4902.
- (19) Lin, Z.; He, Q.; Yin, A.; Xu, Y.; Wang, C.; Ding, M.; Cheng, H. C.; Papandrea, B.; Huang, Y.; Duan, X. Cosolvent Approach for Solution-Processable Electronic Thin Films. *ACS Nano* **2015**, *9*, 4398-405.
- (20) DuBois, M. R. Catalytic Applications of Transition-Metal Complexes with Sulfide Ligands. *Chem. Rev.* **1989**, *89*, 1-9.
- (21) Zaera, F. Nanostructured Materials for Applications in Heterogeneous Catalysis. *Chem. Soc. Rev.* **2013**, *42*, 2746-2762.
- (22) An, K.; Somorjai, G. A. Size and Shape Control of Metal Nanoparticles for Reaction Selectivity in Catalysis. *ChemCatChem* **2012**, *4*, 1512-1524.
- (23) Wei, H.; Liu, X.; Wang, A.; Zhang, L.; Qiao, B.; Yang, X.; Huang, Y.; Miao, S.; Liu, J.; Zhang, T. FeO_x -Supported Platinum Single-Atom and Pseudo-Single-Atom Catalysts for Chemoselective Hydrogenation of Functionalized Nitroarenes. *Nat. Commun.* **2014**, *5*, 1-8.
- (24) Moses-DeBusk, M.; Yoon, M.; Allard, L. F.; Mullins, D. R.; Wu, Z.; Yang, X.; Veith, G.; Stocks, G. M.; Narula, C. K. CO Oxidation on Supported Single Pt Atoms: Experimental and ab Initio Density Functional Studies of CO Interaction with Pt Atom on θ - $Al_2O_3(010)$ Surface. *J. Am. Chem. Soc.* **2013**, *135*, 12634-12645.
- (25) Lin, J.; Qiao, B.; Li, N.; Li, Lin.; Sun, X.; Liu, J.; Wang, X.; Zhang, T. Little Do More: A Highly Effective Pt_1/FeO_x Single-Atom Catalyst for the Reduction of NO by H_2 . *Chem. Commun.* **2015**, *51*, 7911-7914.
- (26) Qiao, B.; Wang, A.; Yang, X.; Allard, L. F.; Jiang, Z.; Cui, Y.; Liu, J.; Li, J.; Zhang, T. Single-Atom Catalysis of CO Oxidation using Pt_1/FeO_x . *Nat. Chem.* **2011**, *3*, 634-641.
- (27) Kistler, J. D.; Chotigkrai, N.; Xu, P.; Enderle, B.; Praserthdam, P.; Chen, C. -Y.; Browning, N. D.; Gates, B. C. A Single-Site Platinum CO Oxidation Catalyst in Zeolite KLTL: Microscopic and Spectroscopic Determination of the Locations of the Platinum Atoms. *Angew. Chem. Int. Ed.* **2014**, *53*, 8904-8907.
- (28) Wickenden, A. E.; Krause, R. A. Polysulfide Chelates. II. Desulfuration of PtS_{15}^{2-} and the Synthesis of PtS_{10}^{2-} . *Inorg. Chem.* **1969**, *8*, 779-783.
- (29) Strasdeit, H.; Krebs, B.; Henkel, G. Synthesis Routes to $[Fe_2X_2(X_5)_2]^{2-}$ Anions (X = S, Se). Structure and Properties of $[Fe_2Se_2(Se_5)_2]^{2-}$, a Complex with Selenido and Pentaselenido Ligands. *Inorg. Chem.* **1984**, *89*, L11-L13.
- (30) Müller, A.; Krickemeyer, E.; Bögge, H.; Clegg, W.; Sheldrick, G. M. $[Ni(S_4)_2]^{2-}$, a Homoleptic Tetrasulfido-Nickel(II) Complex. *Angew. Chem. Int. Ed.* **1983**, *22*, 1006-1007.
- (31) Park, J.; An, K.; Hwang, Y.; Park, J.-G.; Noh, H.-J.; Kim, J.-Y.; Park, J.-H.; Hwang, N.-M.; Hyeon, T. Ultra-Large-Scale Syntheses of Monodisperse Nanocrystals. *Nat. Mater.* **2004**, *3*, 891-895.
- (32) Weidman, M. C.; Beck, M. E.; Hoffman, R. S.; Prins, F.; Tisdale, W. A. Monodisperse, Air-Stable PbS Nanocrystals via Precursor Stoichiometry Control. *ACS Nano* **8**, 6363-6371.
- (33) Zhu, W.; Michalsky, R.; Metin, Ö.; Lv, H.; Guo, S.; Wright, C. J.; Sun, X.; Peterson, A. A.; Sun, S. Monodisperse Au Nanoparticles for Selective Electrocatalytic Reduction of CO_2 to CO. *J. Am. Chem. Soc.* **2013**, *135*, 16833-16836.
- (34) Son, J. S.; Park, K.; Han, M.-K.; Kang, C.; Park, S.-G.; Kim, J.-H.; Kim, W.; Kim, S.-J.; Hyeon, T. Large-Scale Synthesis and Characterization of the Size-Dependent Thermoelectric Properties of Uniformly Sized Bismuth Nanocrystals. *Angew. Chem., Int. Ed.* **2011**, *50*, 1363-1366.
- (35) Son, J. S.; Park, K.; Kwon, S. G.; Yang, J.; Choi, M. K.; Kim, J. Yu, J. H.; Joo, J.; Hyeon, T. Dimension-Controlled Synthesis of CdS Nanocrystals: From 0D Quantum Dots to 2D Nanoplates. *Small* **2012**, *8*, 2394-2402.
- (36) Liu, C.; Wu, X.; Klemmer, T.; Shukla, N.; Weller, D.; Roy, A. G.; Tanase, M.; Laughlin, D. Reduction of Sintering during Annealing of FePt Nanoparticles Coated with Iron Oxide. *Chem. Mater.* **2005**, *17*, 620-625.
- (37) Carbone, L., *et al.* Synthesis and Micrometer-Scale Assembly of Colloidal CdSe/CdS Nanorods Prepared by a Seeded Growth Approach. *Nano Lett.* **2007**, *7*, 2942-2950.
- (38) Dong, A.; Ye, X.; Chen, J.; Kang, Y.; Gordon, T.; Kikkawa, J. M.; Murray, C. B. A Generalized Ligand-Exchange Strategy Enabling Sequential Surface Functionalization of Colloidal Nanocrystals. *J. Am. Chem. Soc.* **2011**, *133*, 998-1006.
- (39) Ban, H. W.; Park, S.; Jeong, H.; Gu, D. H.; Jo, S.; Park, S. H.; Park, J.; Son, J. S. Molybdenum and Tungsten Sulfide Ligands for Versatile Functionalization of All-Inorganic Nanocrystals. *J. Phys. Chem. Lett.* **2016**, *7*, 3627-3635.
- (40) Zhang, L.; He, R.; Gu, H.-C. Oleic acid coating on the monodisperse magnetite nanoparticles. *Appl. Surf. Sci.* **2006**, *253*, 2611-2617.
- (41) Huang, W.; Kuhn, J. N.; Tsung, C. K.; Zhang, Y.; Habas, S. E.; Yang, P.; Somorjai, G. A. Dendrimer templated synthesis of one nanometer Rh and Pt particles supported on mesoporous silica: Catalytic activity for ethylene and pyrrole hydrogenation. *Nano Lett.* **2008**, *8*, 2027-2034.
- (42) Park, J. Y.; Zhang, Y.; Grass, M.; Zhang, T.; Somorjai, G. A. Tuning of Catalytic CO Oxidation by Changing Composition of Rh-Pt Bimetallic Nanoparticles. *Nano Lett.* **2008**, *8*, 673-677.
- (43) Zhang, Z. *et al.* Thermally stable single atom Pt/m- Al_2O_3 for selective hydrogenation and CO oxidation. *Nat. Commun.* **2017**, *8*, 16100.
- (44) An, K.; Alayoglu, S.; Musselwhite, N.; Plamthottam, S.; Melae, G.; Lindeman, A. E.; Somorjai, G. A. Enhanced CO Oxidation Rates at the Interface of Mesoporous Oxides and Pt Nanoparticles. *J. Am. Chem. Soc.* **2013**, *135*, 16689-16696.

SYNOPSIS TOC

